Dynamic Effects on Colloidal Electric Interactions

Y. Ju[†] and J. P. Huang*[,‡]

National Laboratory of Solid State Microstructures and Department of Physics, Nanjing University, Nanjing 210093, China, and Surface Physics Laboratory (National Key laboratory) and Department of Physics, Fudan University, Shanghai 200433, China

Received: December 14, 2007; Revised Manuscript Received: April 12, 2008

Dynamic behaviors are abundant in field-responsive colloidal suspensions. Being beyond the usual point-dipole approximation, we develop a multiple image method of dipoles for two dynamic unequal colloidal dielectric spherical particles, which can be perfectly reduced to those for two static conducting particles. The method is applied to investigate colloidal electric interparticle forces under various conditions of dynamics. As a result, we find that the force can be enhanced, reduced, or even changed from attraction to repulsion, or vice versa. Some other interesting results are also reported. Our theoretical results are compared favorably with existing experimental observations. Therefore, it becomes possible to achieve desired colloidal structures by adjusting colloidal interactions by choosing appropriate dynamic phenomena.

I. Introduction

Colloidal suspensions can be found in many application areas,[1] e.g., paints, inks, pharmaceuticals, food, and brakes. Colloid science and technology plays an important role in some emerging technologies ranging from photonic crystals[2,3] to microfluidics.[4] The macroscopic properties of colloidal suspensions are determined by the microstructure of the particles suspended in the system.[5,6] Dynamic behaviors are abundant in field-responsive colloidal suspensions.[7–9] In the absence of shear, a wide range of stable microstructure in colloidal suspensions can be available in different materials, depending on interparticle forces and Brownian forces. In the presence of shear, the microstructure may depend on the strength of the shear, and it rearranges to accommodate the applied hydrodynamic forces (arising from the shear) and the interparticle and Brownian forces. In fact, when the suspension is subjected to a shear, the microstructure will also affect the rheological properties accordingly. Hence, the intimate coupling between the shear and the microstructure during flow was studied.[10] The relevance lies in the central role of the shear-affected microstructure in determining the macroscopic properties of the suspensions and understanding/controlling the processing behavior of the suspensions with desired microstructures. The competition of different kinds of forces in colloid or complex-fluid systems makes them present variable patterns. Those patterns also provide a way to study the complex relation between the forces. For example, pattern formation has been observed and studied in magnetorheological[11] or electrorheological suspensions.[10,12] Different patterns correspond to their different rheological properties.[13]

The study of colloidal electric interactions is important in understanding or realizing different microstructures of colloidal suspensions.[1,14,15] For instance, if such forces are determined, their macroscopic structures and thus physical properties can be determined. For convenience, we shall focus on the interparticle forces between rotating particles, which is of particular importance in the study of colloidal suspensions including electrorheological fluids, magnetorheological suspensions, living cells suspensions, and so on, since the particles suspended in these fluids may rotate under a shearing flow.[16–25] So far, the investigation of the interparticle force between rotating dielectric particles has received much attention.[7–9,26,27]

Recently Tao and Lan[8] experimentally reported that the rotation of a dielectric particle (polyamide) can significantly reduce the attracting interparticle force between the rotating dielectric particle and a stationary one in argon gas. Also, most recently, we[28] experimentally revealed that the yield stress of the electrorheological fluids, in which the suspended TiO_2 particles are modified with 1,4-butyrolactone molecules, were caused to decrease as the shear rate increases. This apparently showed that the existence of dynamical behaviors arising from the shear flow reduces the strength of interaction between the suspended particles.

To discuss such interparticle forces, early theory is often based on the point-dipole approximation (e.g., see refs 29 and 30). The point-dipole approximation is often adopted in computer simulations[31] because it is simple and easy to use. However, when particles are close enough, being beyond the point-dipole interaction, the interaction arising from multiple image dipoles should be expected to appear and play a significant role. Hence, much work has been done to sort out more accurate models.[32–42] While these models hold for static colloidal particles subjected to an external electric field, in this work we shall develop a multiple image method of dipoles to accurately account for the dynamic effects on the interaction between colloidal particles. To this end, we shall report that, under various conditions of dynamics, the colloidal electric interparticle force can be enhanced, reduced, or even changed from attraction to repulsion, or vice versa. Some of the results will be compared favorably with experimental observations. Therefore, it becomes possible to adjust colloidal interactions and then achieve desired colloidal microstructures by choosing appropriate dynamic phenomena.

The remainder of this paper is organized as follows. In Section II, we obtain the expressions for the interaction force between two dynamic dielectric spherical particles, which include the dynamic effects as well as the effect of multiple image dipoles. This is followed by Section III in which numerical results are presented and our results are compared with some existing

* Corresponding author. E-mail: jphuang@fudan.edu.cn.
[†] Nanjing University.
[‡] Fudan University.

10.1021/jp711741a CCC: $40.75
Published on Web 06/05/2008

experimental results. This paper ends with a discussion and conclusion in Section IV.

II. Formalism

A. Interaction between Two Rotating Dielectric Spheres. Let us consider a dielectric sphere with radius a in a host medium. In the presence of an electric field $\vec{E} = E\hat{z}$ polarization charges are induced on the surface of the sphere, hence it has an induced dipole moment $\vec{p}_1^{(0)} = p_1^{(0)}\hat{z}$ with the magnitude[43]

$$p_1^{(0)} = \frac{2\gamma}{3-\gamma}\varepsilon_2 E a^3 \tag{1}$$

where the parameter $\gamma = (\varepsilon_1 - \varepsilon_2)/(\varepsilon_1 + \varepsilon_2)$ denotes the dielectric contrast, ε_1 is the dielectric constant of the sphere, and ε_2 is the dielectric constant of the host medium.

If the sphere is undergoing a rotational motion with angular velocity $\vec{\omega} = \omega\hat{y}$, the displacement of polarization charges takes place, hence the induced dipole moment rotates under the same angular velocity $\vec{\omega}$. Meanwhile, the dipole moment tends to relax back to its original orientation along the z axis. In this situation, the movement of the dipole moment can be characterized by the following differential equation:[7]

$$\frac{\mathrm{d}\vec{p}_1}{\mathrm{d}t} = \vec{\omega}\times\vec{p}_1 - \frac{1}{\tau}(\vec{p}_1 - \vec{p}_1^{(0)}), \tag{2}$$

where the first term on the right-hand side is due to the rotational motion, and the second term is due to a relaxation process. In eq 2, $p_1^{(0)}$ denotes the static dipole moment of the sphere at rest, and p_1 is the steady (or equilibrium) dipole moment of the sphere in rotation. The relaxation time τ in eq 2 is determined by the details of the relaxation process of the polarized charge distribution on the surface of a rotating sphere, and is generally about 10^{-3} s for a dielectric spherical particle.[8,9] In this work, the dimensionless value $|\omega\tau| = 0-5$ will be used for calculations, which generally corresponds to an applied shear rate of several hundreds (s^{-1}) if the rotation of the sphere is caused to appear by shear flow. The fact that we set $\omega\tau$ as a whole for calculations implies that either ω or τ plays an equivalent role in the dynamic effects as long as $\omega\tau$ is fixed.

When a steady state is reached, we have $\mathrm{d}\vec{p}_1/\mathrm{d}t = \vec{0}$. So far, the dipole moment $\vec{p}_1$ in the steady state can be obtained directly,[7] with the components p_{1x} and p_{1z} along the x and z directions, respectively:

$$p_{1x} = \frac{\omega\tau p_1^{(0)}}{1+(\omega\tau)^2} \tag{3}$$

$$p_{1z} = \frac{p_1^{(0)}}{1+(\omega\tau)^2} \tag{4}$$

Note that the y component of $\vec{p}_1$ is zero (namely, $p_{1y} = 0$) since the angular velocity $\vec{\omega}$ is directed along the y direction. Apparently, both eqs 3 and 4 show that the magnitude of the dipole moment is decreased by a factor of $1/[1+(\omega\tau)^2]^{1/2}$ due to the rotational motion of the sphere, and that the angle between the original dipole moment $\vec{p}_1^{(0)}$ and the steady one $\vec{p}_1$ is

$$\varphi = \arctan(\omega\tau) \tag{5}$$

Then we consider two spheres A and B with radii a and b, respectively. These spheres can both rotate as shown in Figure 1. In order to calculate the total dipole moment $\vec{p}_\mathrm{A}$ or $\vec{p}_\mathrm{B}$ of sphere A or B according to the multiple image method of dipoles (which will be presented in Section II.B), the dipole moment of each sphere $p_{1,\sigma}$ (σ = A or B) should be decomposed into the longitudinal and transverse components, which means that the dipole moment of each sphere is projected to the axis parallel with and perpendicular to the line joining the centers of the two spheres, respectively. Throughout this work, the superscripts L and T will be used to indicate the corresponding parameters in longitudinal and transverse cases, respectively. If the angle between the $\hat{z}$ axis and the center-to-center line is θ (see Figure 1), the longitudinal and transverse components of $\vec{p}_{1,\sigma}$ are respectively

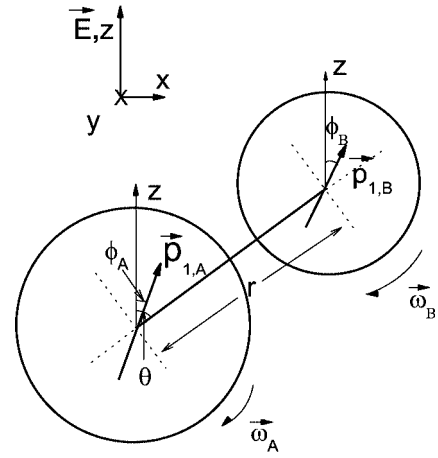

Figure 1. Schematic graph showing a model case of two rotating dielectric spherical particles A and B with angular velocity $\vec{\omega}_\mathrm{A} = \omega_\mathrm{A}\hat{y}$ and $\vec{\omega}_\mathrm{B} = \omega_\mathrm{B}\hat{y}$, respectively. The steady or equilibrium dipole moment $\vec{p}_{1,\mathrm{A}}$ or $\vec{p}_{1,\mathrm{B}}$ of the particle A or B has an angle of ϕ_A or ϕ_B with respect to the z-directed static dipole moment of the resting particle A or B under an electric field $\vec{E} = E\hat{z}$. θ denotes the angle between $\vec{E}$ and the line joining the centers of the particles A and B.

$$p_{1,\sigma}^\mathrm{L} = \frac{p_{1,\sigma}^{(0)}}{\sqrt{1+(\omega_\sigma\tau)^2}}\cos(\theta-\phi_\sigma) \tag{6}$$

$$p_{1,\sigma}^\mathrm{T} = \frac{p_{1,\sigma}^{(0)}}{\sqrt{1+(\omega_\sigma\tau)^2}}\sin(\theta-\phi_\sigma) \tag{7}$$

So far, based on the energy consideration,[38,43] the force between the spheres A and B is given by

$$F_\mathrm{r} = \frac{1}{2}\frac{\mathrm{d}}{\mathrm{d}r}[\vec{E}_\mathrm{A}\cdot\vec{p}_\mathrm{A} + \vec{E}_\mathrm{B}\cdot\vec{p}_\mathrm{B}] \tag{8}$$

$$F_\theta = \frac{1}{2}\frac{\mathrm{d}}{r\mathrm{d}\theta}[\vec{E}_\mathrm{A}\cdot\vec{p}_\mathrm{A} + \vec{E}_\mathrm{B}\cdot\vec{p}_\mathrm{B}] \tag{9}$$

where F_r and F_θ are the radial force and tangential force, respectively. $F_\mathrm{r} > 0$ means that the radial interaction between the two spheres is repulsive, otherwise it is attractive. $F_\theta > 0$ means that the tangential interaction between the two spheres makes the angle θ enlarged, otherwise it is shrunken. In eqs 8 and 9, $\vec{E}_A$ and $\vec{E}_B$ denote the equivalent electrical fields acting on spheres A and B, respectively, which could induce the same dipole moments as $\vec{p}_{1,\mathrm{A}}$ and $\vec{p}_{1,\mathrm{B}}$ if the two rotating spheres were resting. Therefore, the equivalent field should point to the same orientation as the steady dipole moment $\vec{p}_1$ and its magnitude should be $E/[1+(\omega\tau)^2]^{1/2}$. In other words, the induced dipole moment $p_1^{(0)}$ (eq 1) should be always along the direction of the applied electric field $\vec{E} = E\hat{z}$, and the steady dipole moment p_1 (eqs 6 and 7) should be directed along the equivalent field. In case of $\omega = 0$ (static cases), the steady dipole moment p_1 will return to $p_1^{(0)}$, and the equivalent field will return to the applied field $\vec{E} = E\hat{z}$ naturally.

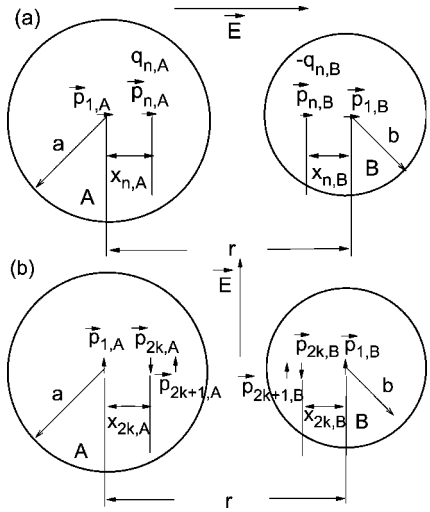

Figure 2. (a) Schematic graph showing images of multidipoles and charges for two unequal dielectric spherical particles A and B under applied electric field $\vec{E}$ that makes the original dipole moment $\vec{p}_1$ parallel with the line joining the centers of the two particles, namely, for a longitudinal field case. Here, r denotes the center-to-center separation, and x_n is the position of the nth order image dipole moment $\vec{p}_n$ and image charge q_n or $-q_n$. The radii of the two particles A and B are a and b, respectively. (b) Same as panel a, but under an applied electric field $\vec{E}$ that makes $\vec{p}_1$ perpendicular to the line joining the centers of the two particles, namely, for a transverse field case. Note that, in either particle A or B, the even-order ($2k$) image dipole moments are antiparallel to $\vec{p}_1$, while the odd-order ($2k + 1$) ones are parallel with $\vec{p}_1$. Meanwhile, there are no image charges.

In eqs 8 and 9, $\vec{E}_A \cdot \vec{p}_A = \vec{E}_A^L \cdot \vec{p}_A^L + \vec{E}_A^T \cdot \vec{p}_A^T$ and $\vec{E}_B \cdot \vec{p}_B = \vec{E}_B^L \cdot \vec{p}_B^L + \vec{E}_B^T \cdot \vec{p}_B^T$. Here, $\vec{E}_{A,B}^{L,T}$ denotes the field component acting on sphere A or B in either the longitudinal (L) or transverse (T) case, which induces the corresponding total dipole moment component $\vec{p}_{A,B}^{L,T}$. Generally, $E_\sigma^L = E/[1+(\omega_\sigma\tau)^2]^{1/2} \cos(\theta - \phi_\sigma)$ and $E_\sigma^T = E/[1+(\omega_\sigma\tau)^2]^{1/2} \sin(\theta - \phi_\sigma)$. In Section II.B, we shall show how to calculate the $\vec{p}_{A,B}^{L,T}$ for two dynamic unequal dielectric spherical particles, by developing a multiple image method of dipoles (see eqs 38–41 below).

B. Multiple Image Dipole Moments for a Pair of Dynamic Unequal Dielectric Spheres. Let us recall some results of image method, and consider a dielectric sphere of dielectric constant ε_1 with radius a suspended in a host medium of dielectric constant ε_2 . If a point charge q is placed at a distance of r ($>a$) with respect to the center of the sphere, the electric potential can be fixed by putting an image charge $q' = -\gamma(a/r)q$ at the position a^2/r with respect to the center of the sphere,[43] where $\gamma = (\varepsilon_1 - \varepsilon_2)/(\varepsilon_1 + \varepsilon_2)$ denotes the dielectric contrast. On the other hand, if a point dipole $\vec{p}$ (which is given by eq 6 or eq 7) is placed at a distance of r ($>a$) with respect to the center of the sphere, the electric potential can also be fixed by putting an image dipole $\vec{p}'$ and an image charge q' at the position a^2/r for large dielectric contrast.[34] The magnitudes of the image dipole and image charge are connected with the angle between the original point dipole $\vec{p}$ and the line joining the centers of the sphere and original point dipole. When the dipole $\vec{p}$ is parallel with the line (longitudinal case), one obtains $\vec{p}' = \gamma(a/r)^3\vec{p}$ and $|q'| = \gamma(a/r^2)p$. In this situation, if the dipole points to the sphere, q' takes a negative charge; if it points away from the sphere, q' takes a positive charge. On the other hand, when the original point dipole $\vec{p}$ is perpendicular to the line (transverse case), $\vec{p}' = -\gamma(a/r)^3\vec{p}$ and $q' = 0$.

Further, let us consider two isolated unequal dielectric spheres A and B, with radii a and b, respectively, as shown in Figure 2a. We use r to denote the center-to-center distance between the two spheres. There are point dipoles $\vec{p}_{1,A}$ ($= p_1^L$ in eq 6 for sphere A) and $\vec{p}_{1,B}$ ($= p_1^L$ in eq 6 for sphere B) in the centers of spheres A and B, respectively. Both dipoles are parallel with the line joining the centers of the two spheres (longitudinal case). The original dipole $\vec{p}_{1,A}$ in sphere A can image a dipole $\vec{p}_{2,B}$ and a charge $q_{2,B}$ in sphere B. The imaged dipole and charge will continue to induce the third dipole $\vec{p}_{3,A}$ and charge $q_{3,A}$ in sphere A. As a result, an infinite series of multidipoles is formed. The nth-order result is

$$p_{n,A} = \gamma\left(\frac{a}{r - x_{n-1,B}}\right)^3 p_{n-1,B} \tag{10}$$

$$q_{n,A} = \frac{\gamma a p_{n-1,B}}{(r - x_{n-1,B})^2} + \frac{\gamma a q_{n-1,B}}{r - x_{n-1,B}} \tag{11}$$

$$x_{n,A} = \frac{a^2}{r - x_{n-1,B}} \tag{12}$$

where $q_{1,A} = 0$ and $x_{1,A} = 0$. Here, $x_{n,A}$ denotes the position of the nth-order image dipole moment $\vec{p}_{n,A}$ and image charge $q_{n,A}$ in sphere A. A similar image process can occur corresponding to the original dipole $\vec{p}_{1,B}$, with

$$p_{n,B} = \gamma\left(\frac{b}{r - x_{n-1,A}}\right)^3 p_{n-1,A} \tag{13}$$

$$q_{n,B} = \frac{\gamma b p_{n-1,A}}{(r - x_{n-1,A})^2} + \frac{\gamma b q_{n-1,A}}{r - x_{n-1,A}} \tag{14}$$

$$x_{n,B} = \frac{b^2}{r - x_{n-1,A}} \tag{15}$$

It is obvious that the odd-order image dipoles and image charges result from the original dipole in the same sphere, but the even-order image dipoles and image charges result from the original dipole in the other sphere. This regulation is very important and will be used in later deduction.

According to eqs 10, 12, 13, and 15, we obtain the following recurrence relation:

$$\frac{r}{p_{n,A}^{1/3}} = \frac{a}{\gamma^{1/3} p_{n-1,B}^{1/3}} + \frac{\gamma^{1/3} b}{p_{n+1,B}^{1/3}} \tag{16}$$

$$\frac{r}{p_{n,B}^{1/3}} = \frac{b}{\gamma^{1/3} p_{n-1,A}^{1/3}} + \frac{\gamma^{1/3} a}{p_{n+1,A}^{1/3}} \tag{17}$$

They can further be rewritten as

$$\frac{r^2 - a^2 - b^2}{ab}\frac{1}{p_{n,A}^{1/3}} = \frac{1}{\gamma^{2/3} p_{n-2,A}^{1/3}} + \frac{\gamma^{2/3}}{p_{n+2,A}^{1/3}} \tag{18}$$

$$\frac{r^2 - a^2 - b^2}{ab}\frac{1}{p_{n,B}^{1/3}} = \frac{1}{\gamma^{2/3} p_{n-2,B}^{1/3}} + \frac{\gamma^{2/3}}{p_{n+2,B}^{1/3}} \tag{19}$$

which can be solved exactly by utilizing the relations $\sinh(n + 2)\vartheta + \sinh(n - 2)\vartheta = 2 \cosh 2\vartheta \sinh n\vartheta$ and $\cosh(n + 2)\vartheta + \cosh(n - 2)\vartheta = 2 \cosh 2\vartheta \cosh n\vartheta$. The solution is

$$p_{n,A}^o = p_{1,A}\gamma^{n-1}\left(\frac{b \sinh 2\vartheta}{a \sinh(n-1)\vartheta + b \sinh(n+1)\vartheta}\right)^3 \tag{20}$$

$$p_{n,A}^e = p_{1,B}\gamma^{n-1}\left(\frac{a \sinh 2\vartheta}{r \sinh n\vartheta}\right)^3 \tag{21}$$

$$p_{n,B}^o = p_{1,B}\gamma^{n-1}\left(\frac{a \sinh 2\vartheta}{b \sinh(n-1)\vartheta + a \sinh(n+1)\vartheta}\right)^3 \tag{22}$$

$$p^{e}_{n,B} = p_{1,A}\gamma^{n-1}\left(\frac{b\sinh 2\vartheta}{r\sinh n\vartheta}\right)^3 \quad (23)$$

where ϑ is defined as $\cosh 2\vartheta = (r^2 - a^2 - b^2)/(2ab)$, the superscript "o" denotes $n = 2k - 1$ (odd-order terms), and "e" represents $n = 2k$ (even-order terms). Combining eqs 10–15 and 20–23, we obtain

$$x^{o}_{n,A} = \frac{ar\sinh(n-1)\vartheta}{a\sinh(n-1)\vartheta + b\sinh(n+1)\vartheta} \quad (24)$$

$$x^{e}_{n,A} = \frac{a^2\sinh n\vartheta + ab\sinh(n-2)\vartheta}{r\sinh n\vartheta} \quad (25)$$

$$x^{o}_{n,B} = \frac{br\sinh(n-1)\vartheta}{b\sinh(n-1)\vartheta + a\sinh(n+1)\vartheta} \quad (26)$$

$$x^{e}_{n,B} = \frac{b^2\sinh n\vartheta + ab\sinh(n-2)\vartheta}{r\sinh n\vartheta} \quad (27)$$

and

$$q^{o}_{n,A} = \frac{p_{1,A}}{a}\gamma^{n-1}\frac{br\sinh 2\vartheta\sinh(n-1)\vartheta}{[a\sinh(n-1)\vartheta + b\sinh(n+1)\vartheta]^2} \quad (28)$$

$$q^{e}_{n,A} = \frac{p_{1,B}}{b}\gamma^{n-1}\frac{a\sinh 2\vartheta(a\sinh(n-2)\vartheta + b\sinh n\vartheta)}{(r\sinh n\vartheta)^2} \quad (29)$$

$$q^{o}_{n,B} = \frac{p_{1,B}}{b}\gamma^{n-1}\frac{ar\sinh 2\vartheta\sinh(n-1)\vartheta}{[b\sinh(n-1)\vartheta + a\sinh(n+1)\vartheta]^2} \quad (30)$$

$$q^{e}_{n,B} = \frac{p_{1,A}}{a}\gamma^{n-1}\frac{b\sinh 2\vartheta(b\sinh(n-2)\vartheta + a\sinh n\vartheta)}{(r\sinh n\vartheta)^2} \quad (31)$$

Since the two dielectric spheres are isolated, two charges $-q_{cA}$ (eq 36) and q_{cB} (eq 37) should be put at the centers of the spheres *A* and *B*, respectively, in order to keep charge neutralization of the dielectric spheres. The two point charges will also induce a series of image charges, whose normalized magnitudes are

$$\lambda^{o}_{n,A} = \gamma^{n-1}\frac{b\sinh 2\vartheta}{a\sinh(n-1)\vartheta + b\sinh(n+1)\vartheta} \quad (32)$$

$$\lambda^{e}_{n,A} = \gamma^{n-1}\frac{a\sinh 2\vartheta}{r\sinh n\vartheta} \quad (33)$$

$$\lambda^{o}_{n,B} = \gamma^{n-1}\frac{a\sinh 2\vartheta}{b\sinh(n-1)\vartheta + a\sinh(n+1)\vartheta} \quad (34)$$

$$\lambda^{e}_{n,B} = \gamma^{n-1}\frac{b\sinh 2\vartheta}{r\sinh n\vartheta} \quad (35)$$

Their positions are the same as those given in eqs 24–27. According to the requirement of charge neutralization, $-q_{cA}$ and q_{cB} can be obtained as

$$q_{cA} = \frac{\sum_{n=1}^{\infty} q_{n,B}\sum_{n=2}^{\infty}\lambda^{e}_{n,A} - \sum_{n=1}^{\infty} q_{n,A}\sum_{n=1}^{\infty}\lambda^{o}_{n,B}}{\sum_{n=2}^{\infty}\lambda^{e}_{n,A}\sum_{n=2}^{\infty}\lambda^{e}_{n,B} - \sum_{n=1}^{\infty}\lambda^{o}_{n,A}\sum_{n=1}^{\infty}\lambda^{o}_{n,B}} \quad (36)$$

$$q_{cB} = \frac{\sum_{n=1}^{\infty} q_{n,A}\sum_{n=2}^{\infty}\lambda^{e}_{n,B} - \sum_{n=1}^{\infty} q_{n,B}\sum_{n=1}^{\infty}\lambda^{o}_{n,A}}{\sum_{n=2}^{\infty}\lambda^{e}_{n,A}\sum_{n=2}^{\infty}\lambda^{e}_{n,B} - \sum_{n=1}^{\infty}\lambda^{o}_{n,A}\sum_{n=1}^{\infty}\lambda^{o}_{n,B}} \quad (37)$$

So far, including all the contribution of dipoles and charges, the total dipole moment can be obtained as

$$p^{L}_{A} = \sum_{n=1}^{\infty} p_{n,A} + \sum_{n=1}^{\infty}(q^{o}_{n,A}x^{o}_{n,A} + q^{e}_{n,A}x^{e}_{n,A}) - \left(\sum_{n=1}^{\infty} q_{cA}\lambda^{o}_{n,A}x^{o}_{n,A} + q_{cB}\lambda^{e}_{n,A}x^{e}_{n,A}\right)$$

$$p^{L}_{B} = \sum_{n=1}^{\infty} p_{n,B} + \sum_{n=1}^{\infty}(q^{o}_{n,B}x^{o}_{n,B} + q^{e}_{n,B}x^{e}_{n,B}) - \left(\sum_{n=1}^{\infty} q_{cB}\lambda^{o}_{n,B}x^{o}_{n,B} + q_{cA}\lambda^{e}_{n,B}x^{e}_{n,B}\right)$$

Or, they can be alternatively written as

$$p^{L}_{A} = \sum_{k=1}^{\infty} p_{k,A} + \sum_{k=1}^{\infty}(q_{2k-1,A}x_{2k-1,A} + q_{2k,A}x_{2k,A}) - \left(\sum_{k=1}^{\infty} q_{cA}\lambda_{2k-1,A}x_{2k-1,A} + q_{cB}\lambda_{2k,A}x_{2k,A}\right) \quad (38)$$

$$p^{L}_{B} = \sum_{k=1}^{\infty} p_{k,B} + \sum_{k=1}^{\infty}(q_{2k-1,B}x_{2k-1,B} + q_{2k,B}x_{2k,B}) - \left(\sum_{k=1}^{\infty} q_{cB}\lambda_{2k-1,B}x_{2k-1,B} + q_{cA}\lambda_{2k,B}x_{2k,B}\right) \quad (39)$$

For the transverse case, in which original point dipoles $\vec{p}_{1,A}$ (= p^{T}_{1} in eq 7 for sphere A) and $\vec{p}_{1,B}$ (= p^{T}_{1} in eq 7 for sphere B) are both perpendicular to the line joining the centers of the two spheres (see Figure 2b), no image charge appears, but the even-order image dipoles point to the opposite direction with respect to the original one. In this case, the total dipole moment is given as

$$p^{T}_{A} = \sum_{n=1}^{\infty}(p^{o}_{n,A} - p^{e}_{n,A}) = \sum_{k=1}^{\infty}(p_{2k-1,A} - p_{2k,A}) \quad (40)$$

$$p^{T}_{B} = \sum_{n=1}^{\infty}(p^{o}_{n,B} - p^{e}_{n,B}) = \sum_{k=1}^{\infty}(p_{2k-1,B} - p_{2k,B}) \quad (41)$$

If the radii of the two dielectric spheres are equal ($a = b$) and the two original dipole moments are also equal ($p_{1,A} = p_{1,B} = p_1$), eqs 20–37 become

$$p_n = p_1\gamma^{n-1}\left(\frac{\sinh\vartheta}{\sinh n\vartheta}\right)^3 \quad (42)$$

$$x_n = a\frac{\sinh(n-1)\vartheta}{\sinh n\vartheta} \quad (43)$$

$$q_n = \frac{p_1}{a}\gamma^{n-1}\frac{\sinh\vartheta\sinh(n-1)\vartheta}{\sinh^2 n\vartheta} \quad (44)$$

$$\lambda_n = \gamma^{n-1}\frac{\sinh\vartheta}{\sinh n\vartheta} \quad (45)$$

$$q_c = \frac{p_1}{a}\sum_{n=1}^{\infty}\gamma^{n-1}\frac{\sinh\vartheta\sinh(n-1)\vartheta}{\sinh^2 n\vartheta}\Big/\sum_{n=1}^{\infty}\gamma^{n-1}\frac{\sinh\vartheta}{\sinh n\vartheta} \quad (46)$$

Therefore, we obtain the expressions for the total dipole moments of each sphere, p^{L} (longitudinal case) and p^{T} (transverse case), as

$$p^{L} = p_1\left[\sum_{n=1}^{\infty}\gamma^{n-1}\left(\frac{\sinh\vartheta}{\sinh n\vartheta}\right)^3 + \sum_{n=1}^{\infty}\gamma^{n-1}\frac{\sinh\vartheta\sinh^2(n-1)\vartheta}{\sinh^3 n\vartheta} - \left(\sum_{n=1}^{\infty}\gamma^{n-1}\frac{\sinh\vartheta\sinh(n-1)\vartheta}{\sinh^2 n\vartheta}\right)^2\Big/\left(\sum_{n=1}^{\infty}\gamma^{n-1}\frac{\sinh\vartheta}{\sinh n\vartheta}\right)\right] \quad (47)$$

$$p^{T} = p_1\sum_{n=1}^{\infty}(-\gamma)^{n-1}\left(\frac{\sinh\vartheta}{\sinh n\vartheta}\right)^3 \quad (48)$$

which have the same forms as eqs 11 and 12 in ref 34, respectively. Here, ϑ satisfies $\cosh\vartheta = r/2a$ (for the case of

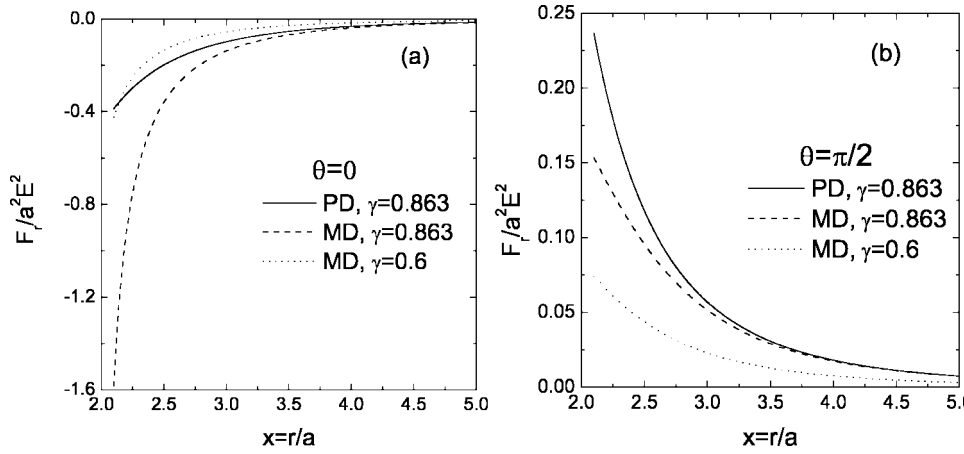

Figure 3. Reduced radial force $F_r/(a^2E^2)$ versus $x = r/a$ for a pair of identical resting dielectric spheres with radius a, for various dielectric contrast γ, for the same configuration as shown in Figure 1 with (a) $\theta = 0$ (namely, longitudinal field case) and (b) $\theta = \pi/2$ (i.e., transverse field case). Here "PD" corresponds to the curves calculated by using the point dipole approximation, and "MD" represents those calculated by using the multiple image method of dipoles.

two identical spheres). Further, if we take the limit $\gamma = 1$ (and $\omega = 0$), they will reduce to the results for static conducting spheres, which are in perfect agreement with the eqs 18 and 10 in ref 39.

Until now, the substitution of eqs 38–41 into eqs 8 and 9 can yield the radial and tangential forces F_r and F_θ between two dielectric spherical particles, by taking into account the dynamic effects as well as the effect of multiple image dipoles. In our theory, the introduction of $\omega\tau$ is just indicative of the existence of the dynamic effects, which comes to appear in eqs 38–41 according to p_1 of eqs 6 and 7.

There have been three steps in our consideration to derive the total dipole moment (eqs38–41): First, give the dipole moment [in eq 1] induced by an applied field for a static sphere. Second, obtain the steady dipole moment (in eqs 6 and 7] for a rotating sphere. Finally, derive the longitudinal and transverse components of the total dipole moment (in eqs 38–41) via the multiple image method of dipoles.

Here we should remark that, when we investigate the dynamic effects, eqs 47 and 48 can not be used. This is because eqs 47 and 48 describe only the situation that the longitudinal or transverse component of dipole moment p in the two spheres is equal to each other. In other words, they are only valid for two stationary identical dielectric spheres under an applied electric field. However, this situation is not satisfied when one or two spheres begin to rotate. For this purpose, eqs 38–41 for two different spheres should be adopted instead. Thus, in all our following calculations, we shall use only eqs 38–41.

III. Results and Discussion

A. Numerical Results. For model calculations, we take two equal-sized spherical particles into account, that is, $a = b$, in an attempt to focus on the effect of dynamics. In addition, we set $\varepsilon_1 = 30$ (dielectric constant of the particles) and $\varepsilon_2 = 2.2$ (dielectric constant of the host medium, e.g., silicone oil), thus yielding $\gamma = 0.86$. In the figures, "PD" corresponds to the curves calculated by using the point dipole approximation, namely, only taking the terms up to $k = 1$[38] in eqs 38–41. In contrast, "MD" means those calculated by the multiple image method of dipoles, i.e., taking all the terms up to $k = \infty$ in eqs 38–41.

Figure 3 shows the reduced radial force $F_r/(a^2E^2)$ as a function of $x = r/a$ with various dielectric contrasts γ for a pair of resting dielectric spheres, for the same configuration as shown in Figure 1 with (a) $\theta = 0$ (namely, longitudinal field case for which the radial force is attractive) and (b) $\theta = \pi/2$ (i.e., transverse field case for which the radial force is repulsive). In general, it is observed that smaller separation x leads to larger radial force, and the magnitude of the attractive force is larger than that of the repulsive force at fixed separation x . Further, we find that, for the longitudinal (or transverse) field case, the attractive (or repulsive) interaction predicted by the multiple image method of dipoles is stronger (or weaker) than that obtained from the point-dipole approximation. The result corresponding to the longitudinal field case can be understood conveniently from Figure 2a, in which the induced image dipole moments $\vec{p}_n$ ($n \geq 2$) appear parallel to the original dipole moment $\vec{p}_1$, thus enhancing the total dipole moment and thus the attractive interaction. However, for the transverse field case, the even-order (or odd-order) image dipole moments $\vec{p}_{2k}$ (or $\vec{p}_{2k+1}$) are antiparallel (or parallel) to the original dipole moment $\vec{p}_1$, as shown in Figure 2b. The magnitude of $\vec{p}_{2k}$ is generally larger than that of $\vec{p}_{2k+1}$ at certain k . Thus, the total dipole moment is reduced, and thus the repulsive interaction is caused to be reduced accordingly in the multiple image method of dipoles for the transverse field case. On the other hand, we also calculate with $\gamma = 0.6$ and $\varepsilon_2 = 2.2$, and find that the interaction could be caused to increase as the dielectric contrast γ between the particles and host increases.

Figure 4 displays the reduced radial force $F_r/(a^2E^2)$ against $|\omega\tau|$ at different separations $x = r/a$ for a pair of particles, one sphere rotating and the other resting, for the same configuration as shown in Figure 1 with (a,b) $\theta = 0$ (longitudinal field case) and (c,d) $\theta = \pi/2$ (transverse field case). Here, the use of $|\omega\tau|$ implies that, because of the presence of symmetry, the same results can be obtained as the rotating particle rotates either clockwise or anticlockwise. For the longitudinal field case (Figure 4a), the radial force decreases with the increase of rotating angular velocity ω. That is, the attractive interaction between the two particles is weakened due to the effect of dynamics. For the transverse field case (Figure 4c), the behavior somehow becomes complicated. The starting repulsive inter-particle force decreases quickly and disappears at a certain ω, then the force changes to be attractive as ω increases step by step. The reason of the force quality change lies in the following fact: When one particle begins to rotate, a longitudinal component of dipole moment appears, which can contribute a larger attractive force than the repulsive force yielded by a transverse dipole component with the same magnitude. Hence

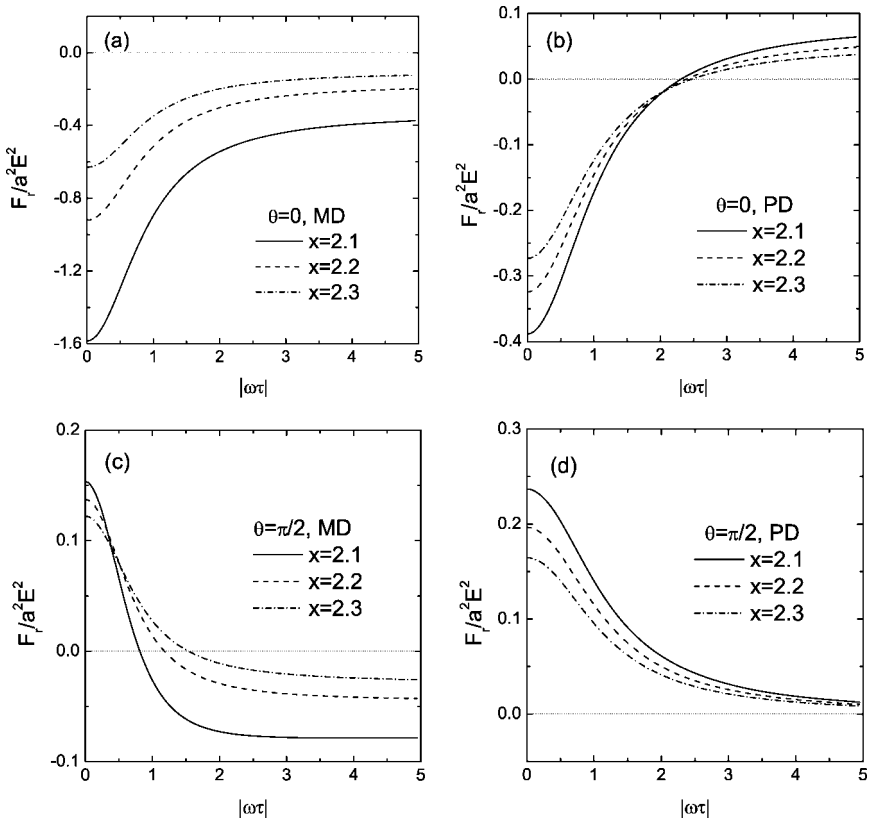

Figure 4. Reduced radial force $F_r/(a^2E^2)$ versus $|\omega\tau|$ (product of angular velocity ω and relaxation time τ) for two identical dielectric spherical particles with radius a, one of which is rotating and the other of which is resting, at different $x = r/a$, for the same configuration as shown in Figure 1 with (a,b) $\theta = 0$ (namely, longitudinal field case) and (c,d) $\theta = \pi/2$ (i.e., transverse field case). Here, the use of $|\omega\tau|$ implies that, because of the presence of symmetry, the same results can be achieved as the rotating particle rotates either clockwise (i.e., $\vec{\omega} = \omega\hat{y}$) or anticlockwise (namely, $\vec{\omega} = -\omega\hat{y}$). "PD" corresponds to the curves calculated by using the point dipole approximation, and "MD" refers to those calculated by using the multiple image method of dipoles.

the change of force quality can take place at a certain ω . On the other hand, at small ω region, the repulsive force is stronger for small particle separations than for large particle separations, which echoes Figure 3 and Figure 4a. However, as ω proceeds to increase, the repulsive force can become weaker for small separations. In a word, while the effect of dynamics may change the magnitude of interparticle forces, it can also be used to change the force from attraction to repulsion, or vice versa.

Figure 5 shows the case of the two particles both rotating with the same angular velocity ω . Figure 5a gives a framework that is similar to that of Figure 4a, but the attractive radial force can be reduced more rapidly and tends to zero in Figure 5a. The reason is that the longitudinal dipole component will decrease more rapidly when both particles rotate. On the other hand, Figure 5c also shows a framework similar to that of Figure 4c, but there is a peak of attractive radial force in the larger ω region. This further shows that the effect of different kinds of dynamics can affect interparticle forces significantly.

Figure 6 plots the case of the two particles rotating oppositely. Figure 6a investigates the longitudinal field case, which gives a result similar to that of either Figure 4a or Figure 5a. However, Figure 6c shows a much different behavior from what Figure 4c and Figure 5c display. The repulsive interparticle force is caused to decrease as either angular velocity ω or separation x increases. It is because when particles rotate oppositely, the longitudinal dipole component in each particle points to an opposite orientation, and hence yields a repulsive radial force. In this case, the quality change of radial force can not take place.

In Figures 4–6, the predictions by the point-dipole approximation are generally different from those by the multiple image method of dipoles. Actually, for very close separations, the multiple image method of dipoles should be more accurate because the former (or the latter) includes (or ignores) the effect of multiple image dipoles. On the other hand, if the separation is large enough, the point-dipole approximation can hold the same as the multiple image method of dipoles, as expected. This is because the effect of multiple image dipoles will become small enough to be neglected. In this case, one may prefer to use the point-dipole approximation due to its simple use and compact form.

Figure 7 displays the reduced tangential force $F_\theta/(a^2E^2)$ versus θ/π, for (a) the case in which particle A is rotating clockwise and particle B is resting; (b) the case in which particle A is rotating anticlockwise and particle B is resting; (c) the case in which both particles A and B are rotating clockwise; and (d) the case in which both particles A and B are rotating anticlockwise. In all the four panels, the case of both resting particles [$\omega\tau = 0$(A); 0(B)] is also plotted for comparison. This figure clearly shows that, for two resting particles, there is no tangential force ($F_\theta = 0$) for either the longitudinal field case ($\theta = 0$) or the transverse field case ($\theta = \pi/2$). The dashed curve and dash-dotted curve describe the results for the cases in which one particle or both particles begin to rotate. It is obvious that larger angular velocity leads to smaller tangential interparticle force. For the convenience of analysis, in each panel we use three small circles to indicate the same phase points corresponding to $F_\theta = 0$ at (a,c) $\theta \geq 0$ and (b,d) $\theta < 0$. (In fact, for the opposite region of θ, there are also another series of the same phase points corresponding to $F_\theta = 0$. However, the analysis is the same as below.) We find that the orientation of the

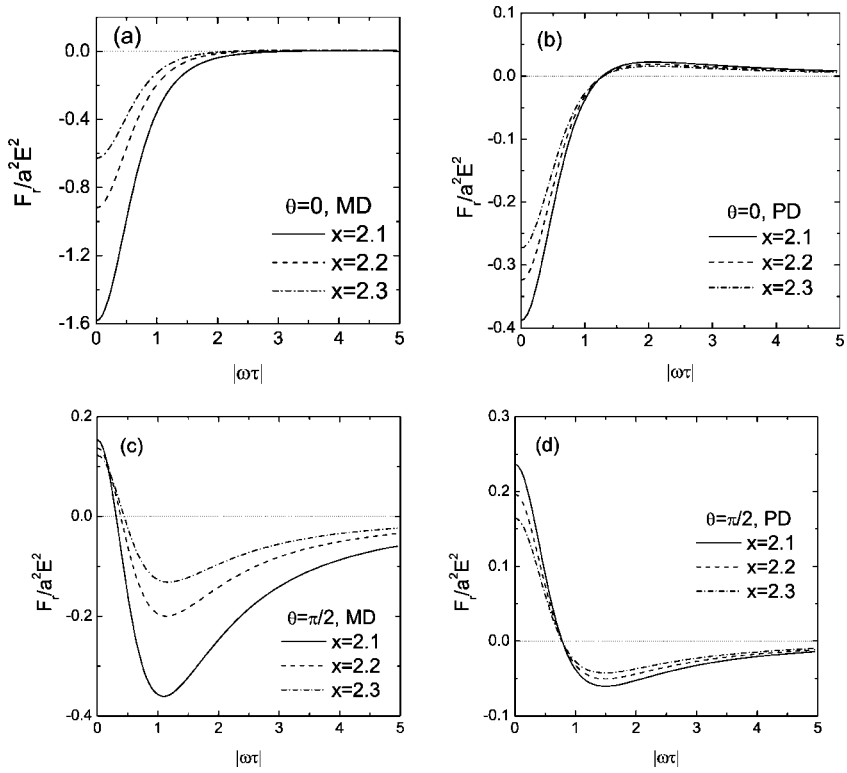

Figure 5. Same as Figure 4, but both of the two particles are rotating with the same angular velocity, either $\vec{\omega} = \omega\hat{y}$ or $\vec{\omega} = -\omega\hat{y}$.

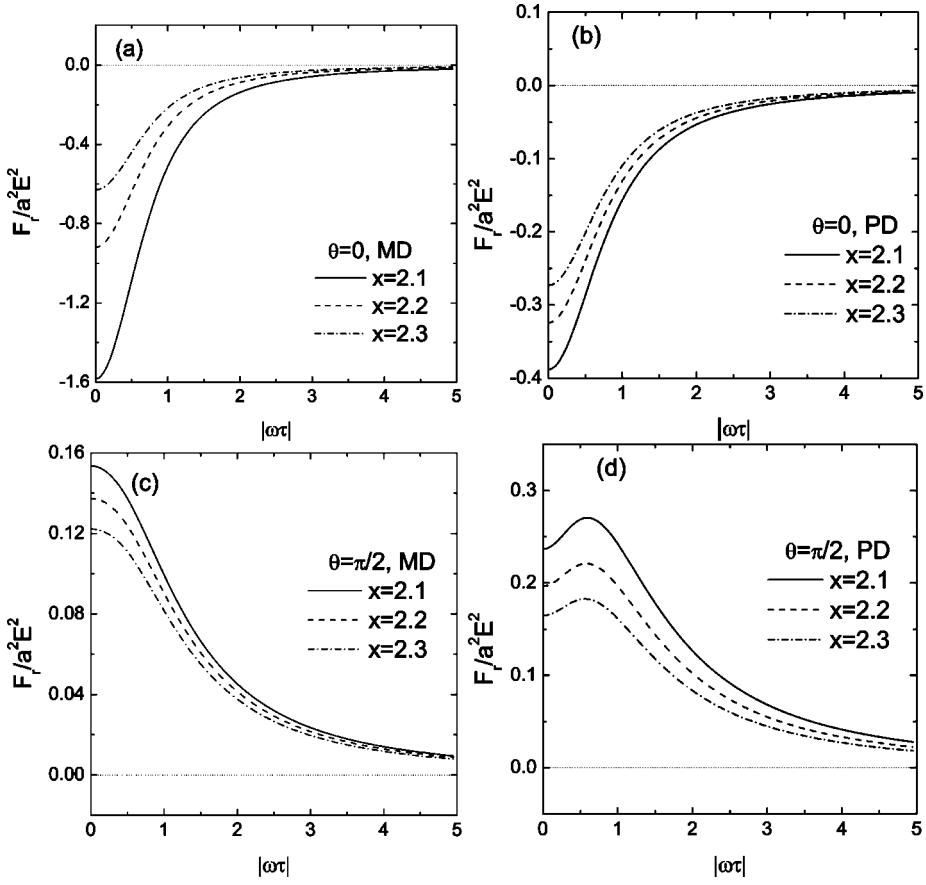

Figure 6. Same as Figure 4, but the two particles are rotating oppositely, one of which corresponds to $\vec{\omega} = \omega\hat{y}$, and the other of which is $\vec{\omega} = -\omega\hat{y}$.

tangential force changes according to the variance of the orientation of the dipole moment due to particle rotation. In other words, when a dielectric sphere rotates clockwise (or anticlockwise), the angle between the steady dipole moment and applied electric field will be $\phi > 0$ (or $\phi < 0$), and the same phase points move to an angle of $\theta > 0$ (or $\theta < 0$)

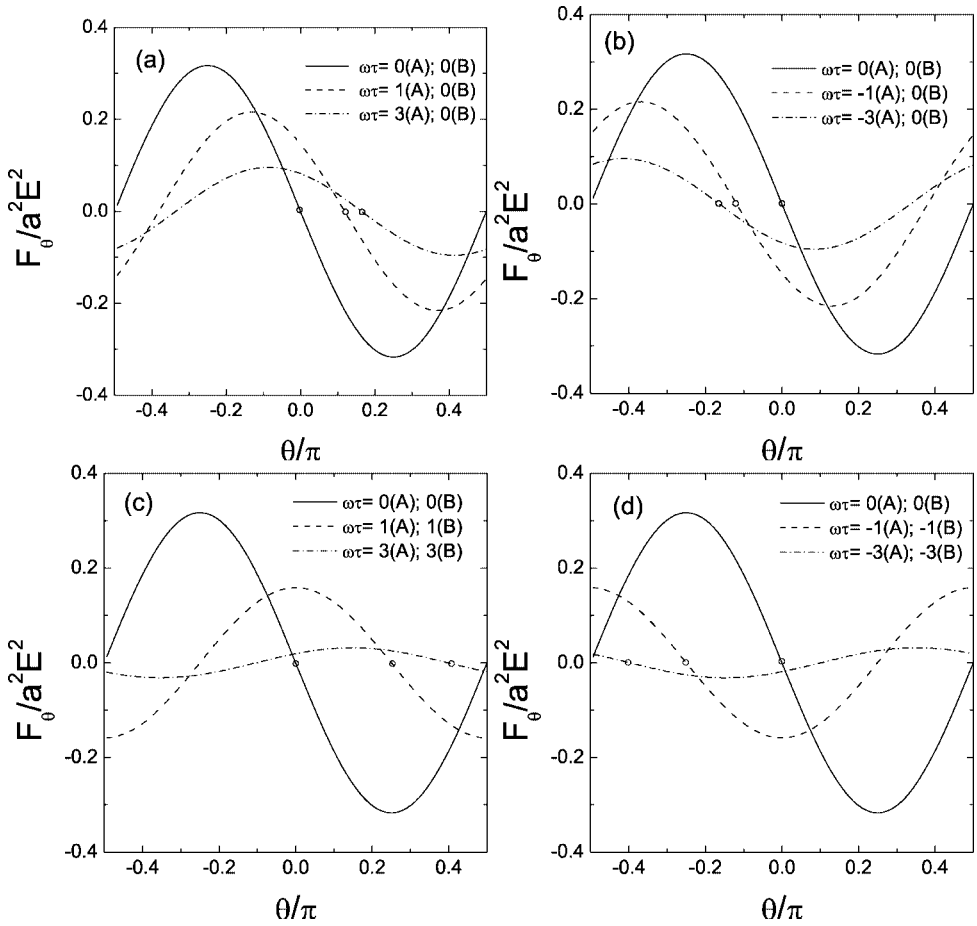

Figure 7. Reduced tangential force $F_\theta/(a^2E^2)$ versus θ/π, for (a) the case in which particle A is rotating clockwise and particle B is resting [$\omega\tau = 1$(A); 0(B) and $\omega\tau = 3$(A); 0(B)]; (b) the case in which particle A is rotating anticlockwise and particle B is resting [$\omega\tau = -1$(A); 0(B) and $\omega\tau = -3$(A); 0(B)]; (c) the case in which both particles A and B are rotating clockwise [$\omega\tau = 1$(A); 1(B) and $\omega\tau = 3$(A); 3(B)]; and (d) the case in which both particles A and B are rotating anticlockwise [$\omega\tau = -1$(A);-1(B) and $\omega\tau = -3$(A);-3(B)]. All the four panels also display the case of both resting particles [$\omega\tau = 0$(A); 0(B)]. In each panel, three small circles are used to indicate the same phase points corresponding to $F_\theta = 0$ at (a,c) $\theta \geq 0$ and (b,d) $\theta < 0$. All the curves in this figure are calculated by using the multiple image method of dipoles.

accordingly (see panel a (or b) of Figure 7). In particular, when both particles rotate with the same angular velocity (Figure 7c,d), these same phase points move to $\theta = \phi = \arctan(\omega\tau)$.

B. Comparison with Some Experimental Observations. Tao and Lan[8] experimentally studies two touching dielectric spherical particles (polyamide), one of which is resting and the other of which is rotating. They reported that, for the longitudinal field case, increasing the rotating angular velocity decreases the interparticle force between the two particles, which favorably echoes our predictions obtained from Figure 4a.

Recently, we[28] fabricated a kind of polar-molecules-modified electrorheological fluid, in which TiO_2 particles modified by 1,4-butyrolactone molecules are suspended in silicone oil. For such systems, we experimentally investigated the yield stress versus shear rate, and found that the increase of shear rate causes shear stress to be decreased. Apparently, this is due to the rotation of the suspended particles. In fact, such rotation causes the reduction of the polarization of the particles. These experimental results qualitatively agree with the present theoretical results obtained from Figures 4a, 5a, and 6a.

IV. Conclusion

In this work, the expressions for the dipole moments of two unequal dielectric spherical particles in three dimensions have been obtained in the multiple image method of dipoles. In so doing, a point dipole is introduced at the center of each sphere, and successive image dipoles are introduced to maintain the boundary conditions. As a matter of fact, it follows a similar way to develop the same method for treating the dipole moments of two unequal cylindrical or circular particles in two dimensions (see the Appendix). In two dimensions this image process is exact and yields an exact infinite-series representation of the induced dipole moments. Nevertheless, in three dimensions the process yields an asymptotic approximation valid for very large dielectric contrasts.

For colloidal particles suspended in electric-field-responsive colloidal suspensions, there are mainly two kinds of interactions, namely, electric interactions and hydrodynamical interactions. (Actually, there are also other existing interactions such as the Browian interaction and the van der Waals interaction.) In this work we focus only on electric interactions between colloidal particles. Regarding the hydrodynamical interactions, for two spherical particles, a commonly used method is the reflection method,[44] which is similar to the multiple image method of dipoles in electrics. In principle, the reflection method can be developed to investigate the hydrodynamic interaction between two rotating particles, or between a rotating particle and a stationary one. But, as far as we know, no explicit work has been done in this direction (which is also out of the scope of this work). Nevertheless, we can estimate that, besides the separation between two suspended particles, the viscous torque of a particle plays also a key role in the hydrodynamic

interaction. In general, larger viscous torque and/or smaller separation yields stronger hydrodynamic interaction. However, their quantitative relation with hydrodynamic interaction is subjected to future research. Here it is worth mentioning that, for an isolated spherical (colloidal) particle with diameter D less than 500 μm, the laminar viscous torque Γ may be invoked as $\Gamma = \pi\eta D^3\omega$,[45] where η denotes the viscosity of the host liquid.

To summarize, being beyond the usual point-dipole approximation, we have developed a multiple image method of dipoles to accurately calculate the electric interaction between two dynamic colloidal dielectric particles. We have also further applied them to investigate various conditions of dynamics, and found that the colloidal electric interparticle force can be enhanced, reduced, or even changed from attraction to repulsion, or vice versa. Our theoretical results are compared favorably with some existing experimental observations. Therefore, it becomes possible to obtain various colloidal structures by adjusting colloidal interactions by choosing appropriate dynamic phenomena.

Acknowledgment. We thank Mr. W. J. Tian for helpful discussions. This work was supported by the State Key Program for Basic Research of China under Grant No. 2006CB921803, by the National Natural Science Foundation of China under Grant No. 10604014, by CNKBRSF under Grant No. 2006CB921706, by the Pujiang Talent Project (No. 06PJ14006) of the Shanghai Science and Technology Committee, and by the Shanghai Education Committee ("Shu Guang" Project).

Appendix: A Multiple Image Method of Dipoles for a Pair of Unequal Dielectric Cylinders or Circles

If a point dipole $\vec{p}$ is put in front of a dielectric cylinder or circle (in two dimensions), the electric potential can be fixed by only introducing an image dipole with magnitude $\vec{p}' = \pm\gamma(a/r)^2\vec{p}$ (here, the sign "+" is used for longitudinal cases and "−" is used for transverse cases). In this case, no point charges are needed to keep boundary conditions and charge neutralization.

Let us consider two dielectric cylinders or circles. Their radii are respectively a and b, and the distance between their centers is denoted as r. There is a point dipole moment $\vec{p}_{1,A}$ or $\vec{p}_{1,B}$ in each center, which is parallel with the line joining the centers of the two cylinders or circles (namely, longitudinal cases). Similar to the three-dimensional cases as discussed above, the image process yields an infinite series of image dipoles. As a result, the nth-order result for cylinder or circle A is

$$p_{n,A} = \gamma\left(\frac{a}{r - x_{n-1,B}}\right)^2 p_{n-1,B} \tag{49}$$

$$x_{n,A} = \frac{a^2}{r - x_{n-1,B}} \tag{50}$$

and that for cylinder or circle B can simply be obtained by exchanging the subscripts A and B and replacing a with b. For saving space, we shall omit the corresponding expressions for cylinder or circle B. Next, the recurrence relation should be

$$\frac{r}{p_{n,A}^{1/2}} = \frac{a}{\gamma^{1/2}p_{n-1,B}^{1/2}} + \frac{\gamma^{1/2}b}{p_{n+1,B}^{1/2}} \tag{51}$$

$$\frac{r}{p_{n,B}^{1/2}} = \frac{b}{\gamma^{1/2}p_{n-1,A}^{1/2}} + \frac{\gamma^{1/2}a}{p_{n+1,A}^{1/2}} \tag{52}$$

The solutions of the above equations are

$$p_{n,A}^{o} = p_{1,A}\gamma^{n-1}\left(\frac{b\sinh 2\vartheta}{a\sinh(n-1)\vartheta + b\sinh(n+1)\vartheta}\right)^2 \tag{53}$$

$$p_{n,A}^{e} = p_{1,B}\gamma^{n-1}\left(\frac{a\sinh 2\vartheta}{r\sinh n\vartheta}\right)^2 \tag{54}$$

where ϑ is given by $\cosh 2\vartheta = (r^2 - a^2 - b^2)/(2ab)$, the superscript "o" denotes odd-order terms, and "e" represents even-order terms. So far, the total dipole moment for cylinder or circle A is written as

$$p_A^L = \sum_{n=1}^{\infty} p_{n,A} \tag{55}$$

for longitudinal cases. Similarly, it is given by

$$p_A^T = \sum_{n=1}^{\infty} (p_{n,A}^{o} - p_{n,A}^{e}) \tag{56}$$

for transverse cases.

Finally, for two identical cylinders or circles (i.e., $a = b$ and $p_{1,A} = p_{1,B} = p_1$), eqs 55 and 56 reduce to

$$p^L = p_1\sum_{n=1}^{\infty}\gamma^{n-1}\left(\frac{\sinh\vartheta}{\sinh n\vartheta}\right)^2 \tag{57}$$

$$p^T = p_1\sum_{n=1}^{\infty}(-\gamma)^{n-1}\left(\frac{\sinh\vartheta}{\sinh n\vartheta}\right)^2 \tag{58}$$

which agree very well with eqs 10 and 12 in ref 34.

References and Notes

(1) Hiemenz, P. C.; Rajagopalan, R. *Principles of Colloid and Surface Chemistry*, 3rd ed.; Dekker: New York, 1997.
(2) Vlasov, Y. A.; Yao, N.; Norris, D. J. *Adv. Mater.* **1999**, *11*, 165.
(3) Tao, R.; Xiao, D. *Appl. Phys. Lett.* **2002**, *80*, 4702.
(4) Terray, A.; Oakey, J.; Marr, D. W. M. *Science* **2002**, *296*, 1841.
(5) Larson, R. G. *Rheology and Structure of Complex Fluids*; Oxford University Press: Oxford, 1999.
(6) For example, see Wei, E. B.; Dong, L.; Yu, K. W *J. Appl. Phys.* **2006**, *99*, 054101.
(7) Wan, J. T. K.; Yu, K. W.; Gu, G. Q. *Phys. Rev. E* **2001**, *64*, 061501.
(8) Tao, R.; Lan, Y. C. *Phys. Rev. E* **2005**, *72*, 041508.
(9) Tian, W. J.; Liu, M. K.; Huang, J. P. *Phys. Rev. E* **2007**, *75*, 021401.
(10) Cao, J. G.; Huang, J. P.; Zhou, L. W. *J. Phys. Chem. B* **2006**, *110*, 11635.
(11) Cutillas, S.; Bossis, G.; Cebers, A. *Phys. Rev. E* **1998**, *57*, 804.
(12) Sun, J. M.; Tao, R. *Phys. Rev. E* **1996**, *53*, 3732.
(13) Henley, S.; Filisko, F. E. *Int. J. Mod. Phys. B* **2002**, *16*, 2286.
(14) Delville, A. *J. Phys. Chem. B* **2005**, *109*, 8164.
(15) Zhang, H.; Lu, H. Y.; Hu, N. F. *J. Phys. Chem. B* **2006**, *110*, 2171.
(16) Halsey, T. C. *Science* **1992**, *258*, 761.
(17) von Pfeil, K.; Graham, M. D.; Klingenberg, D. J.; Morris, J. F. *Phys. Rev. Lett.* **2002**, *88*, 188301.
(18) Wen, W.; Huang, X.; Yang, S.; Lu, K.; Sheng, P. *Nat. Mater.* **2003**, *2*, 727.
(19) Jiang, Y.; Liu, M. *Phys. Rev. Lett.* **2004**, *93*, 148001.
(20) Hove, J. R.; Koster, R. W.; Forouhar, A. S.; Acevedo-Bolton, G.; Fraser, S. E.; Gharib, M. *Nature (London)* **2003**, *421*, 172.
(21) Tzima, E.; Irani-Tehrani, M.; Kiosses, W. B.; Dejana, E.; Schultz, D. A.; Engelhardt, B.; Cao, G. Y.; DeLisser, H.; Schwartz, M. A. *Nature (London)* **2005**, *437*, 426.
(22) Wang, Y.; Dimitrakopoulos, P. *Phys. Rev. Lett.* **2006**, *96*, 028106.
(23) Misbah, C. *Phys. Rev. Lett.* **2006**, *96*, 028104.
(24) Huang, J. P. *Phys. Rev. E* **2004**, *70*, 041403.
(25) Huang, J. P. *Phys. Rev. E* **2004**, *70*, 042501.
(26) Gu, G. Q.; Yu, K. W.; Hui, P. M. *J. Chem. Phys.* **2002**, *116*, 24.
(27) Wan, J. T. K.; Yu, K. W.; Gu, G. Q. *Phys. Rev. E* **2002**, *62*, 6846.
(28) Xu, L.; Tian, W. J.; Wu, X. F.; Cao, J. G.; Zhou, L. W.; Huang, J. P.; Gu, G. Q. *J. Mater. Res.* **2008**, *23*, 409.
(29) Tao, R.; Sun, J. M. *Phys. Rev. Lett.* **1991**, *67*, 398.
(30) Brioude, A.; Pileni, M. P. *J. Phys. Chem. B* **2005**, *109*, 23371.
(31) Klingenberg, D. J.; Swol, F. V.; Zukoski, C. F. *J. Chem. Phys.* **1991**, *94*, 6160.
(32) Poladian, L. *Q. J. Mech. Appl. Math.* **1988**, *41*, 395.

(33) Klingenberg, D. J.; Swol, F. V.; Zukoski, C. F. *J. Chem. Phys.* **1991**, *94*, 6170.
(34) Poladian, L. *Phys. Rev. B* **1991**, *44*, 2092.
(35) Davis, L. C. *Appl. Phys. Lett.* **1992**, *60*, 319.
(36) Clercx, H. J. H.; Bossis, G. *Phys. Rev. E* **1993**, *48*, 2721.
(37) Djordjević, B. R.; Hetherington, J. H.; Thorpe, M. F *Phys. Rev. B* **1996**, *53*, 14862.
(38) Yu, K. W.; Wan, J. T. K. *Comput. Phys. Commun.* **2000**, *129*, 177.
(39) Jiang, Z.; Shen, Z.; Lu, K. *J. Electrost.* **2001**, *53*, 53.
(40) Jiang, Z. *J. Electrost.* **2003**, *58*, 247.
(41) Bruzzone, S.; Malvaldi, M.; Arrighini, G. P.; Guidotti, C. *J. Phys. Chem. B* **2005**, *109*, 3807.
(42) Avramopoulos, A.; Papadopoulos, M. G.; Reis, H. *J. Phys. Chem. B* **2007**, *111*, 2546.
(43) Jackson, J. D. *Classical Electrodynamics*, 3rd ed.; John Wiley & Sons, Inc.: New York, 2001.
(44) Happel, J.; Brenner, H. *Low Reynolds Number Hydrodynamics*; Kluwer Academic: Dordrecht/Boston/London, 1983.
(45) Lamb, H. *Hydrodynamics*; Dover Press: New York, 1945.

JP711741A